Nacre-like composites with superior specific damping performance

PNAS RESEARCH ARTICLE | ENGINEERING

Nacre-like composites with superior specific damping performance

Wilhelm Woigk[a], Erik Poloni[b], Madeleine Grossman[c], Florian Bouville[c], Kunal Masania[a,1,2], and André R. Studart[a,1]

Edited by Ulrike Wegst, Northeastern University, Boston, MA; received October 14, 2021; accepted June 21, 2022 by Editorial Board Member Joanna Aizenberg

Biological materials such as nacre have evolved microstructural design principles that result in outstanding mechanical properties. While nacre's design concepts have led to bio-inspired materials with enhanced fracture toughness, the microstructural features underlying the remarkable damping properties of this biological material have not yet been fully explored in synthetic composites. Here, we study the damping behavior of nacre-like composites containing mineral bridges and platelet asperities as nanoscale structural features within its brick-and-mortar architecture. Dynamic mechanical analysis was performed to experimentally elucidate the role of these features on the damping response of the nacre-like composites. By enhancing stress transfer between platelets and at the brick/mortar interface, mineral bridges and nano-asperities were found to improve the damping performance of the composite to levels that surpass many biological and man-made materials. Surprisingly, the improved properties are achieved without reaching the perfect organization of the biological counterparts. Our nacre-like composites display a loss modulus 2.4-fold higher than natural nacre and 1.4-fold more than highly dissipative natural fiber composites. These findings shed light on the role of nanoscale structural features on the dynamic mechanical properties of nacre and offer design concepts for the manufacturing of bio-inspired composites for high-performance damping applications.

nacre | bio-inspired materials | hierarchical structures | extreme damping

Significance

Nacre has inspired scientists because of its ability to reach high stiffness and fracture toughness using relatively weak mineral building blocks. Suppressing vibration is another remarkable feature of nacre that has been less explored and is yet to be translated into synthetic composites. We unveil the damping principles of tough biological materials by investigating structure-property relationships of model nacre-like composites. Our bio-inspired structures display a loss modulus 2.4-fold higher than natural nacre and 1.4-fold higher than lightweight flax-based composites used for damping applications, despite the less organized brick-and-mortar architecture compared to nacre. Since such properties arise primarily from the multiscale structure of the material, this work opens an enticing pathway toward high-performance composites using more sustainable, environmentally friendly building blocks.

Nacre is well known for its remarkable fracture toughness (1–5). The toughness of this biological material relies on the unique arrangement of inorganic platelets and organic biopolymer in a so-called brick-and-mortar architecture. Because the platelets and the biopolymer alone are inherently weak and soft, nacre offers a unique example of how microstructural design can be exploited to reach outstanding mechanical properties. This has motivated researchers to create biologically inspired composites that replicate some of the structural design principles of nacre and thus produce materials with enhanced mechanical performance or more sustainable resources (6–9). Nanoscale features of the brick-and-mortar structures, such as platelet-connecting mineral bridges and nano-asperities on the platelet surface, were found to be crucial for the high fracture toughness of nacre (5, 10–12). While extensive research has been dedicated to unveiling the design principles underlying the high fracture toughness of nacre, much less is known about the dynamic properties, in particular the damping behavior, of nacre and nacre-like composites.

Damping is essential for the safe operation and for vibration control in many modern technologies and structures, including earthquake-proof buildings (13), structural parts of aerospace vehicles (14), and motion control systems (15). Since they are exposed to high mechanical loads, structures used in these applications also need materials with high stiffness. Combining damping and stiffness is a challenging task, because these properties are often antagonistic in a single material. Composites can be designed to circumvent the usual damping-stiffness trade-off, making them attractive choices for such applications (16). Metal-matrix composites are known to display exceptional damping performance (17–21), which can be described using several physical models (22, 23). In the case of polymer-based composites, laminates of stiff and soft multilayers (24) and polymers reinforced with flax fibers (25) are typical examples of lightweight composites that exploit high shear strains in dissipative phases of their microstructure to enhance the damping response. Notably, nacre displays specific damping behavior comparable to the best-performing synthetic composites (26–31). However, the design principles responsible for such high damping performance are not yet fully understood.

Recent micromechanical models suggest that the damping properties of biological materials, such as bone and nacre, rely on their staggered platelet architecture (32–35). Upon mechanical loading, a staggered arrangement of stiff elements in a soft matrix leads

The authors declare no competing interest.

This article is a PNAS Direct Submission. U.G.W. is a Guest Editor invited by the Editorial Board.

[1]To whom correspondence may be addressed. Email: k.masania@tudelft.nl or andre.studart@mat.ethz.ch.

[2]Present address: Shaping Matter Lab, Faculty of Aerospace Engineering, Delft University of Technology, 2629 HS Delft, Netherlands.

This article contains supporting information online at http://www.pnas.org/lookup/suppl/doi:10.1073/pnas.2118868119/-/DCSupplemental.

Published July 25, 2022.

to stress transfer between platelets and shear within the polymer matrix. The mechanical properties of such model composite is dominated either by the stiff platelets or the soft matrix, depending on the level of overlap between platelets, their aspect ratio, and the material properties of the constituent phases (23, 32). Under matrix-dominated conditions, the model predicts a simultaneous increase in stiffness and dissipation upon increasing stress transfer between the stiff platelets. Recent experiments have confirmed this prediction in platelet-reinforced polymers with a nacre-inspired structure (26). Despite the unusual set of mechanical properties achieved, the relatively low volume fraction of stiff platelets in the polymer (up to 30 vol%) has limited the damping performance of the composite. Moreover, the role of nanoscale structural features such as mineral bridges and nanoscale asperities on the damping performance of biological nacre and nacre-like composites has not yet been investigated.

Here, we study the effect of mineral bridges and nanoscale asperities on the damping behavior of nacre-like composites. Using a magnetic-assisted manufacturing process, nacre-like composites with high volume fraction of platelets and variable nanoscale structural features were prepared and experimentally evaluated. The fractions of mineral bridges and nano-asperities generated under different manufacturing conditions were assessed by image analysis of the nacre-like microstructures. Dynamic mechanical analysis was conducted to quantify the damping properties of the composites and correlate them with the nanoscale structural features. Finally, the damping performance of our nacre-like composites is compared to those of other synthetic and biological reference materials.

Nacre-like composites were manufactured using the previously reported vacuum-assisted magnetic alignment (VAMA) technique (Fig. 1*A*) (36, 37). In this approach, anisotropic particles suspended in a liquid are first assembled into an aligned structure by performing vacuum-assisted filtration under an external rotating magnetic field. When platelet-shaped particles are used, the rotating frequency of the applied magnetic field is tuned to ensure the biaxial alignment of the suspended platelets parallel to the bottom of the filter (38, 39). The magnetically assembled structure is then subjected to a hot-pressing process at temperatures in the range 700–1,000 °C to obtain a porous, mechanically stable brick-and-mortar scaffold. In this step, the volume fraction of particles in the assembly is increased and strong interconnections between the particles are built. Finally, the pores of the hot-pressed scaffold are infiltrated with a reactive liquid resin, which is thermally polymerized to generate the nacre-like composite.

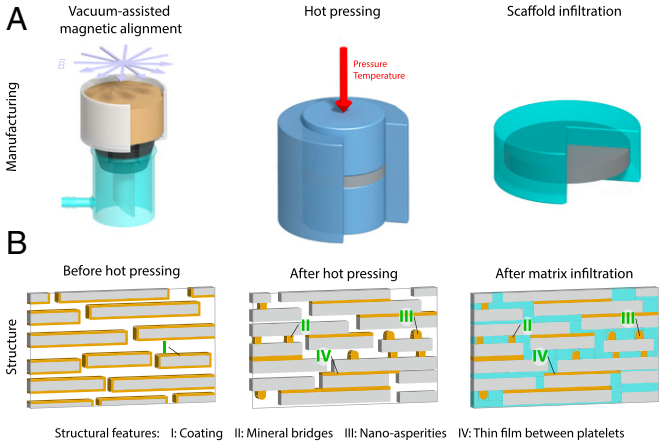

Fig. 1. Manufacturing and structural features of nacre-like composites. (*A*) Schematics of the VAMA process used to generate brick-and-mortar architectures with high volume fraction of inorganic platelets. (*B*) Illustration of the structural features formed within the brick-and-mortar architecture upon dewetting of the titania coating from the surface of the alumina platelets.

In order to prepare nacre-like composites with nanoscale structural features, we use titania-coated alumina platelets as anisotropic particles in the VAMA process. Such platelets are rendered magnetic-responsive by suspending them in water and electrostatically adsorbing superparamagnetic iron oxide nanoparticles (SPIONs) on their surface to enable field-induced alignment. The titania coating is crucial to create the nacre-like nanoscale features. During the hot-pressing step, this coating undergoes dewetting from the alumina surface, leading to the formation of titania mineral bridges and nano-asperities between and on the surface, respectively, of the platelets within the brick-and-mortar structure (Fig. 1*B*). Importantly, the mineral bridges and nano-asperities are not disturbed during the subsequent infiltration process, resulting in a unique nacre-like microstructure after the final polymerization step.

The volume fraction of inorganic phase and the density of mineral bridges and nano-asperities formed in the nacre-like structure depend directly on the temperature and pressure applied during the hot-pressing step. To systematically study the effect of mineral bridges and nano-asperities on the mechanical properties of the nacre-like composites, we selected temperature/pressure conditions that lead to a constant inorganic phase fraction of 60 vol% after hot-pressing (40). A constant pressure of 20 MPa was required to reach this volume fraction of solids in the scaffold pressed up to 800 °C. Above this temperature, partial softening of the titania phase led to a reduction of this critical pressure needed to achieve 60 vol% solids, as the pressing temperature was increased. This resulted in the following sets of temperature/pressure conditions for the preparation of the isodense scaffolds: 700 °C/20 MPa, 750 °C/20 MPa, 800 °C/20 MPa, 850 °C/17.5 MPa, 900 °C/15 MPa, and 1,000 °C/5 MPa.

Scanning electron microscopy (SEM) images of the cross-sections of scaffolds processed at these different conditions provide important insights into the evolution of the brick-and-mortar microstructure for increasing temperatures (Fig. 2 *A*–*C*). High temperatures are crucial to promote dewetting of the titania layer from the alumina platelet, thus enabling the formation of mineral bridges, nano-asperities or interplatelet thin films. In specimens pressed at 800 °C or below, we found that the dewetting process leads predominantly to the formation of mineral bridges. Such bridges result from the dewetting of the titania coating from platelets in close proximity. For higher processing temperatures in the range 800–900 °C, both mineral bridges and nano-asperities are observed. Nano-asperities emerge when adjacent platelets are too far to establish a mineral bridge upon dewetting of the titania coating. Increasing the temperature to 1,000 °C caused extensive clustering of the platelets and partial distortion of the initial brick-and-mortar structures. This likely results from high capillary forces acting on the relatively soft titania phase. Such microstructural changes follow a similar trend to that reported in our earlier study (36).

To better evaluate these qualitative trends and quantify the density of nanoscale features for the distinct scaffolds, we performed image analysis on specimens prepared at different temperatures. Following our earlier work (40), image analysis was used to measure the size of the titania features observed within the brick-and-mortar microstructures (Fig. 2 *D*–*F*). The size of the titania features provides a simple way to differentiate between the different possible nanoscale structures present in the scaffold. Features smaller than 75 nm correspond to titania coatings in low-temperature specimens and thin films between platelets for high-temperature samples. Mineral bridges are identified

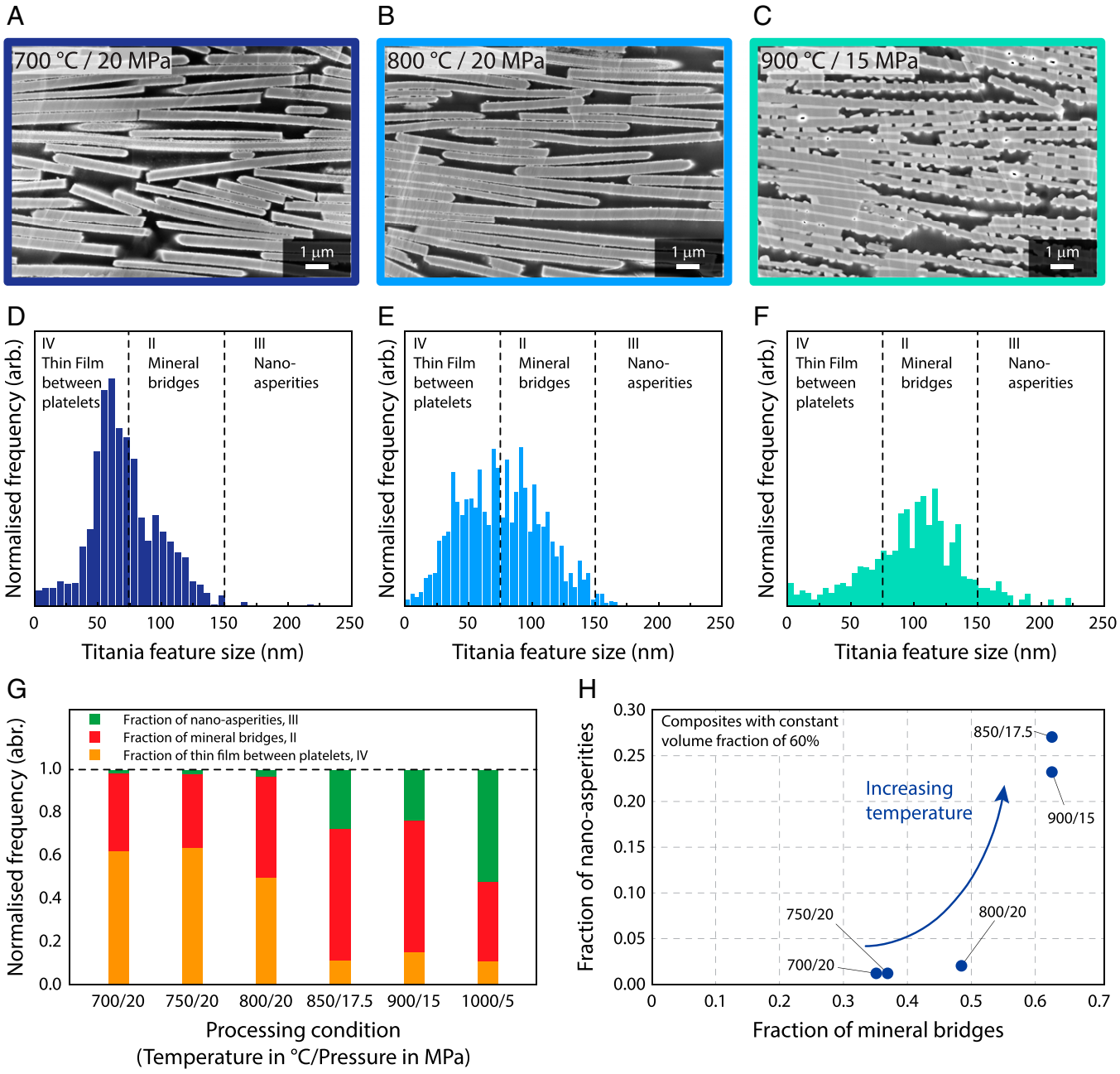

Fig. 2. Microstructural analysis of scaffolds used for the manufacturing of nacre-like composites. (*A–C*) Representative SEM images of scaffolds obtained by hot-pressing assembled platelets under distinct temperatures and pressures. (*D–F*) Size distribution of titania features obtained by image analysis and used to estimate the fractions of mineral bridges and nano-asperities within the brick-and-mortar structures. (*G*) Fraction of mineral bridges, nano-asperities, and thin films or coatings of specimens prepared at different temperatures and pressures. (*H*) Observed experimental correlation between the fraction of mineral bridges and of nanoscale asperities in the investigated composites. The temperature and pressure used to fabricate the scaffolds are provided for each data point.

from titania features between 75 and 150 nm in size. Finally, titania feature sizes larger than 150 nm are assigned to nanoscale asperities. The frequency of titania features within these specific size ranges was divided by the total number of detected features to obtain the fraction of nanoscale structural elements in every specimen (*SI Appendix*).

Our microstructural analysis reveals that the fraction of mineral bridges gradually increased from 0.36 to 0.62 as the processing temperature is increased up to 900 °C (Fig. 2*G*). Notably, this trend is accompanied by an increase of the fraction of nano-asperities from 0.01 to 0.23 within the same temperature range (Fig. 2*H*). Such structural features are formed at the expense of titania coatings and interplatelet thin films, the fraction of which decreases from 0.62 to 0.11 when the temperature is increased from 700 °C to 900 °C. The platelet clustering effect observed in samples pressed at 1,000 °C was found to affect predominantly the relative ratio between mineral bridges and nano-asperities. This ratio drops from 4.1 for specimens processed at 900 °C to 3.5 for samples prepared at 1,000 °C.

The ability to systematically vary the microstructure of the brick-and-mortar scaffolds while keeping the inorganic phase content fixed opens the possibility to study the effect of structural features on the damping behavior of nacre-like composites. To this end, scaffolds prepared at different temperature/pressure conditions were infiltrated and polymerized to generate a series of nacre-like specimens for mechanical testing (*SI Appendix*, Fig. S1). The damping properties of samples pressed at temperatures

ranging from 700 and 900 °C were characterized by dynamic mechanical analysis (DMA) using a three-point-bending configuration. The response of the nacre-like composites to an oscillating mechanical stress was quantified in terms of the storage modulus (E'), the loss modulus (E″) and the dissipation factor (tan (δ) = E''/E'). Independent cyclic tests in a universal mechanical testing machine showed that the maximum strain applied during DMA lies within the linear viscoelastic regime of the material, suggesting that the mineral bridges and nanoasperities are not damaged during the dynamic analysis (*SI Appendix*, Fig. S2). The fact that the storage modulus of the nacre-like composites does not depend on the frequency applied in the DMA supports this interpretation (*SI Appendix*, Fig. S3).

The experimental results show that composites prepared from scaffolds pressed at 850 °C, 900 °C, and 1,000 °C display higher storage modulus, loss modulus and dissipation factor in comparison to the samples obtained at lower temperatures (700 °C, 750 °C, and 800 °C, Fig. 3 *A*–*C*). The simultaneous increase in stiffness (E') and damping losses (tan (δ)) for specimens processed at higher temperatures is remarkable in view of the usual trade-off observed for these two mechanical properties. Importantly, the high volume fraction of inorganic phase of these composites (60 vol%) leads to stiffness levels that are 6.3-times higher compared to previously reported nacre-inspired composites containing 30 vol% platelets (26).

Besides the higher volume fraction of inorganic phase, our nacre-like composites clearly benefit from the formation of nanoscale features within the brick-and-mortar structure. The evaluation of the independent effects of these structural features on the mechanical properties of the composites is challenging because they tend to vary simultaneously upon increasing processing temperature (Fig. 2*H*). Therefore, the possible roles of mineral bridges and nano-asperities on the storage modulus, loss modulus and dissipation factor of the brick-and-mortar structures are discussed here in light of earlier studies on similar nacre-like composites.

The damping properties of nacre-like composites have been theoretically investigated using shear lag micromechanical models applied to staggered platelet architectures (32, 34, 35, 41). Numerical simulations have also been performed to predict the dynamic mechanical properties of brick-and-mortar architectures with different constituent properties (42). While the influence of mineral bridges and nano-asperities have not been explicitly considered, the theoretical models provide insights into the role of other related microstructural parameters, such as the aspect ratio (ρ) and the overlap length between platelets (L). For a given set of material properties, the storage modulus of brick-and-mortar composites generally increases with ρ and L, since larger aspect ratios and interplatelet overlap length enhance stress transfer to the stiff elements of the staggered

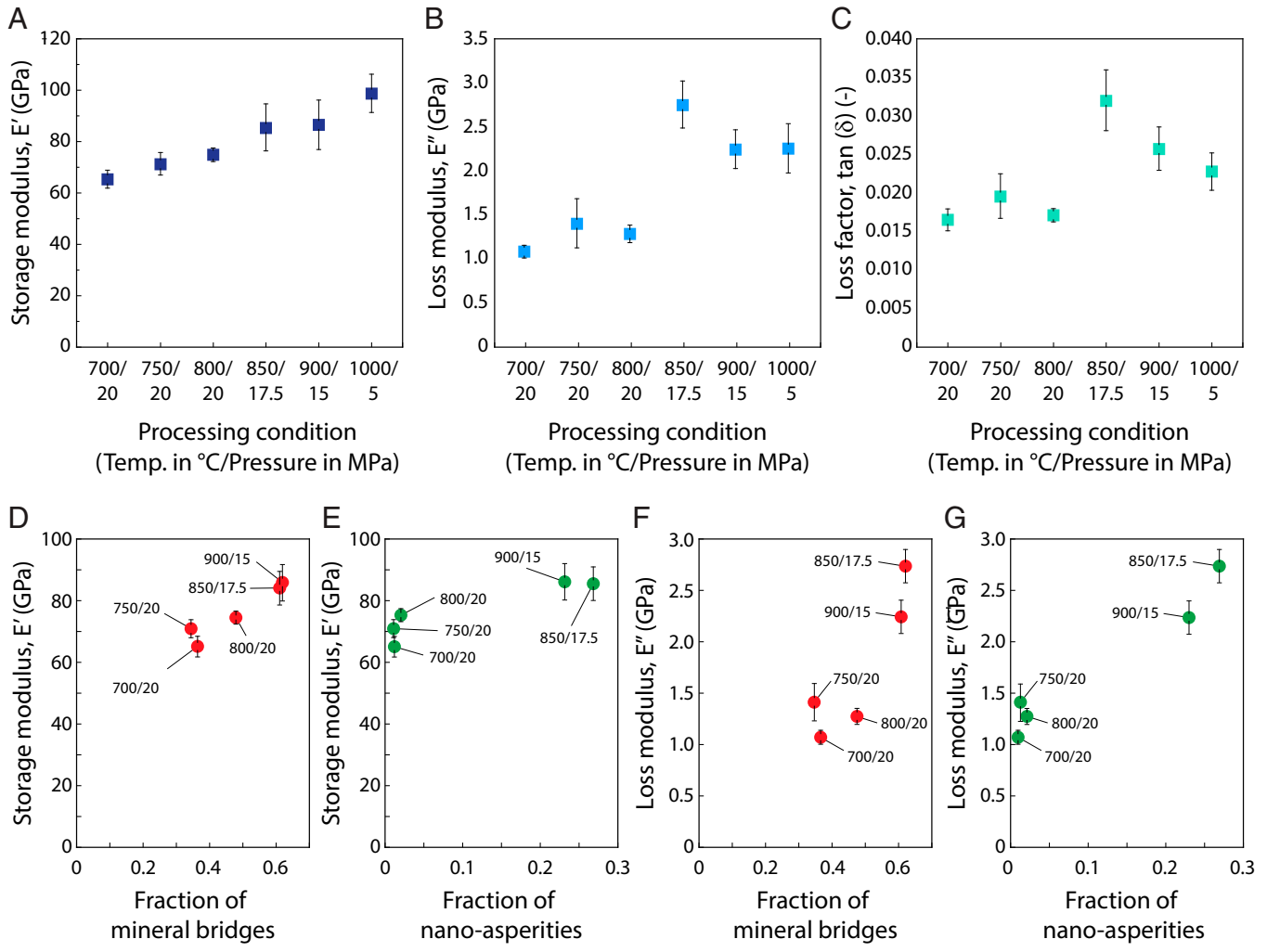

Fig. 3. Damping behavior of nacre-like composites. (*A*) Storage modulus (E'), (*B*) loss modulus (E'') and (*C*) dissipation factor (tan (δ)) of specimens processed at different temperatures and pressures. (*D*–*G*) Experimental correlations between the (*D*, *E*) storage modulus and (*F*, *G*) the loss modulus of the nacre-like composites with the fractions of mineral bridges and nano-asperities.

structure. In contrast, the loss modulus of such architectures shows a maximum at a critical aspect ratio (ρ_c) or critical overlap length (L_c). For $L > L_c$ (or $\rho > \rho_c$), the mechanical properties are dominated by the stiff platelets of the composite. Conversely, the soft matrix controls the mechanical response when $L < L_c$ (or $\rho < \rho_c$). In the soft-dominated regime, theory predicts that both the storage and loss modulus increase with L and ρ.

Since mineral bridges and nano-asperities are expected to increase stress transfer between platelets and at the platelet/matrix interface, we hypothesize that these structural features should have a similar effect as the aspect ratio and the interplatelet overlap length on the mechanical properties of the composites. Plotting the storage and loss modulus data against the fraction of mineral bridges and nano-asperities reveals experimental correlations that support this hypothesis (Fig. 3 *D*–*G*). The more efficient stress transfer in the presence of mineral bridges has been proposed in earlier micromechanical studies (11) and is in good agreement with previously reported experimental data on similar nacre-like composites (40). The mineral bridges are expected to distribute local strains over a larger number of platelets, thereby increasing the total platelet-matrix interface that is subjected to vibration. This in turn enhances the level of interfacial friction and the associated viscoelastic dissipation in the polymer matrix. Nano-asperities should promote stress transfer by enhancing the shear stresses at the platelet-matrix interface through increased friction or interlocking mechanisms, an effect that has also been considered in earlier modeling work (10). The increased interfacial shear stresses directly translate into higher energy dissipation in the polymer phase. Overall, the experimentally observed increase in loss modulus for specimens containing larger fractions of mineral bridges and nano-asperities suggest that the dynamic properties of our composites are dominated by the soft polymer matrix.

To compare the damping behavior of the nacre-like composites with that of other structural materials, we display our experimental data on an Ashby plot together with previously reported results (Fig. 4). The reference materials include biological composites, such as nacre, bone and wood, as well as platelet-reinforced polymers inspired by nacre. Data for flax-based natural composites known for their outstanding damping performance are also depicted in the diagram, along with results from metal-ceramic composites with exceptionally high damping response. Because damping materials used in structural applications need to be simultaneously stiff and dissipative, we use the product E' tan (δ) as a figure of merit for the damping performance. This product is numerically equivalent to the loss modulus (E''), which is therefore taken as performance indicator in our comparison.

The Ashby plot indicates that the nacre-like composites with high fraction of mineral bridges and nano-asperities outcompete many synthetic and natural materials in terms of damping performance. With a loss modulus (E'') of 2.74 GPa, the composites processed at 850 °C perform 5.3-times better in comparison to high-damping flax fiber-reinforced laminates, while still keeping a high storage modulus of 83 GPa. Notably, these remarkable properties do not depend on the loading direction within the plane of aligned platelets. Such in-plane isotropic response is a major advantage compared to the highly anisotropic mechanical properties of the unidirectionally reinforced flax-based composites considered in the analysis. While the out-of-plane properties are challenging to measure due to the relatively small sample size, the strong alignment of platelets within the plane should result in significantly lower composite elastic modulus along the direction transverse to the platelets.

Because it contains alumina platelets that are 3.3-times stiffer than calcium carbonate bricks, the E'' value of our best composite is 2.4-fold higher than that of natural nacre, which has the highest storage modulus among the biological composites. Like nacre and other biological materials, the dissipative properties of our composite are higher than what would be expected by a simple rule of mixture model (5). This is evident when the loss modulus of the best-performing nacre-like composite (2.74 GPa) is compared to the values for the epoxy (60 MPa) and alumina (<100 MPa) constituent phases. While the temperature is expected to affect the dissipative response of the epoxy phase, the inorganic scaffolds can potentially be infiltrated with other polymers to tune the damping performance of the composite according to the temperature of the aimed application. Our comparative analysis reveal that the performance of the nacre-like architectures is also not far from those of highly damping metal-ceramic composites, especially when compared in terms of

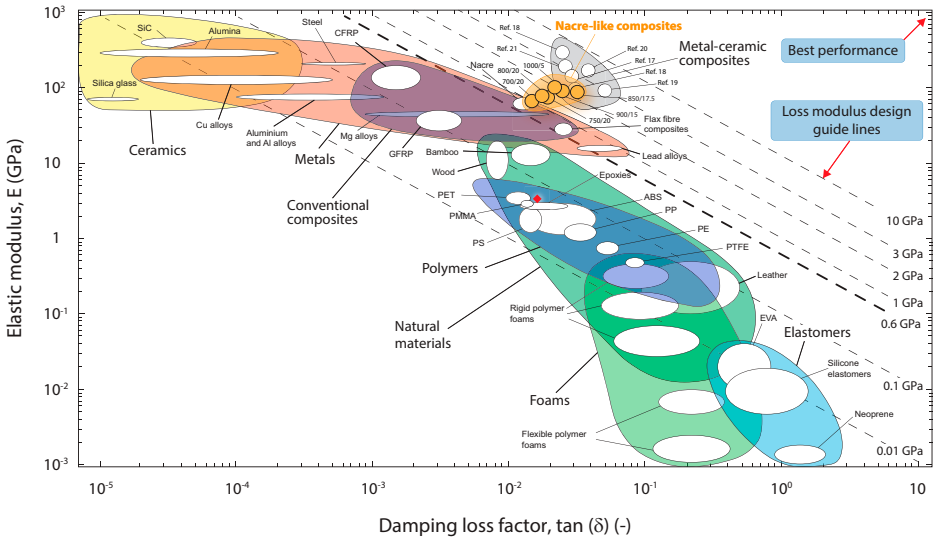

Fig. 4. Ashby plot displaying the stiffness and damping properties of the nacre-like composites (orange circles) compared to other classes of materials. The dashed lines represent the loss modulus, the damping figure of merit, E''. Data were obtained from Lakes (45), CES EduPack (46) and Woigk et al. (26) The room-temperature mechanical properties of the epoxy used for the preparation of the nacre-like composites studied in this work are also included in the plot (red diamond symbol, E' = 3.6 GPa, E'' = 59.7 MPa, tan (δ) = 0.017).

specific properties (*SI Appendix*, Fig. S4). The ability to achieve this set of properties without a metal phase is an interesting feature that may allow for the future fabrication of other nacre-like materials that combine high damping performance with insulating properties or optical transparency (43, 44).

The high damping performance of the composites developed in this study illustrates the effectiveness of mineral bridges and nano-asperities in enhancing mechanical properties that are often antagonistic in synthetic materials. Fine-tuning these nanoscale structural features or implementing them in metal-ceramic composites may lead to bio-inspired materials with further improved damping behavior.

In summary, the incorporation of mineral bridges and nano-asperities in brick-and-mortar structures with a high volume fraction of platelets (60 vol%) enables the fabrication of nacre-like composites with unprecedented damping performance. The enhanced damping behavior of such composites results from the ability of mineral bridges and nano-asperities to increase stress transfer between platelets and at the platelet–matrix interface, respectively. Because the mechanical properties of the composites are dominated by the soft polymer matrix, the improved stress transfer enables a simultaneous increase of the storage and loss modulus of the structure. Such a behavior contrasts with the antagonistic relationship between stiffness and energy dissipation typically found in conventional synthetic materials. By experimentally demonstrating the potential of mineral bridges and nano-asperities in enhancing stiffness and dissipative losses, this study places materials in an unexplored area of the Ashby design diagram and sheds light into another unique design concept of mollusk shells. Importantly, the implementation of such design concept in the bioinspired composite is sufficient to improve its mechanical properties even if the artificial material lacks the perfect brick-and-mortar arrangement of nacre. In future work, the combination of this experimental platform with multiscale analytical tools (47), numerical modeling (48, 49) and machine learning techniques (50) should provide useful guidelines for the manufacturing of next-generation composites with ultra-high damping performance.

Materials and Methods

Materials. Titania-coated alumina microplatelets (Xirallic Crystal Silver T-50, Merck GmbH) were made magnetically responsive through the electrostatic surface adsorption of superparamagnetic iron oxide nanoparticles (SPIONs), as described by Erb et al. (37). Dry magnetized platelets (20 g, 5 vol%) were suspended by vigorous stirring in a 100 mL aqueous solution containing 2% poly(vinyl alcohol) (MW = 13–23 kDa, Sigma Aldrich), 1% poly(acrylic acid) sodium salt (MW = 8 kDa, Polysciences). The resulting suspension was stirred for 24 h to avoid platelet agglomeration. One drop of an antifoaming agent (Antifoam 204, Sigma Aldrich) was added 5 min prior to the magnetic alignment step used to prepare the aligned scaffolds for sintering.

VAMA. Inorganic scaffolds with aligned alumina platelets were produced using the VAMA approach reported in our earlier work (36, 40). To prepare the aligned scaffolds for the subsequent sintering and resin infiltration steps, the platelet suspension was cast into the funnel of the vacuum filtration set-up. The funnel was equipped with filter paper to allow for a sealed system under the weight of the suspension. The setup was encircled by four solenoids that were externally controlled to generate an in-plane rotating magnetic field. A distinct color change was observed 30 seconds after the start of the VAMA process. Since the platelets became more reflective when oriented, this color shift indicates their alignment within the plane of the rotating magnetic field. The aligned platelets were subsequently consolidated into a disk-shaped compact (46 mm diameter) by pulling vacuum at 100 mbar for 25 min. The vacuum led to the removal of excess liquid of the suspension, leading to a mechanically stable scaffold after drying.

Drying and Sintering. Aligned scaffolds were prefired in air at 500 °C for 3 h to remove the organic phase before transferring to a spark plasma sintering (SPS) oven (HP D 10, FCT Systeme GmbH). Samples were sintered in a 50-mm nitrogen-purged graphite die at varying temperatures and pressures. Processing conditions were optimized to achieve nacre-like composites with a platelet volume fraction of 60% (40). To this end, the following temperature/pressure (°C/MPa) combinations were used in this study: 700/20, 750/20, 800/20, 850/17.5, 900/15, and 1,000/5. Depending on those combinations, heating rates between 29 and 40 °C/min were used to reach the final temperature. Once the maximum temperature was reached, a temperature dwell of 10 min was used to allow for microstructural features to arise. This step at constant temperature was followed by a cooling step at 100 °C/min. These heating and cooling rates ensured stable crack-free scaffolds after the sintering process.

Matrix Infiltration. The infiltration of the inorganic scaffold was carried out in an oil-bath press (KIP 100E) that allows for the application of isostatic pressure. For pressing, a sintered scaffold and a commercial epoxy (Sikadur-300) were placed in an evacuated minigrip bag, which was wrapped by a nitrile bag to prevent resin leakage. The final pressing force of 800 kN was reached by gradually increasing the force in 100-kN increments including a dwell time of 30 s. This method was found to be crucial to avoid damaging of the scaffold through excessive build-up of pressure. To ensure complete impregnation, 800 kN pressing force was applied for 10 min. The infiltrated scaffolds were then placed in silicone molds filled with degassed liquid resin and were subsequently oven cured at 70 °C for 5 h under vacuum. This resulted in a porosity of <0.2% in the final infiltrated scaffolds.

Mechanical Characterization. Dynamic mechanical analysis (DMA) was performed using a three-point bending setup with a 20 mm span (Q800 instrument, TA Instruments). The specimens were preloaded with a flexural force of 0.1 N to conduct the measurement in the positive deflection regime. Frequency sweeps were carried out with a frequency range of 1–100 Hz at constant amplitude of 10 μm. The storage modulus E', the loss modulus, E'' and the loss factor, tan (δ), were calculated as the mean obtained from a total of six measurements for each sample configuration. Here, the viscoelastic properties at 10 Hz were extracted and considered for the comparison.

Microscopy and Image Analysis. Quantification of titania feature sizes was performed by image analysis of scanning electron micrograph (SEM) cross sections. Cross sections for microstructural analysis were flat polished with a broad ion beam (BIB) mill (IM4000, Hitachi) and imaged using a scanning electron microscope (GeminiSEM 450, Zeiss). To better differentiate the alumina platelets, the titania coating and the epoxy matrix, the samples were not coated before imaging. This led to a strong contrast between the bright alumina platelets and the dark epoxy phase. Images were prepared for quantitative analysis using the threshold, median and erode functions of the Fiji software package (51). Eight 8-bit images obtained through this process were combined to a cluster of images and the thickness of high-contrast areas determined using Fiji's local thickness function (52). Thicknesses were categorized in a histogram with a bin number of 50. Considering the magnification of the SEM image, the feature sizes could be computed in nanometer scale, which allowed for the assignment of the four titania feature types: unconnected continuous coatings, mineral bridges (connected asperities), nano-asperities (unconnected asperities), and thin films between platelets. The proportion of mineral bridges and thin films between platelets with respect to all the titania features was taken as the fraction of mineral bridges (γ_{mb}), whereas the fraction of nano-asperities (γ_{asp}) was considered to be the proportion of unconnected asperities relative to all the titania features (*SI Appendix*).

Data Availability. All study data are included in the article and/or the *SI Appendix* or avaliable from the authors upon request.

ACKNOWLEDGMENTS. We thank the Gebert Rüf Stiftung (GRS-077/15), the Innosuisse funding programme (18848.1) and the Swiss Competence Center for Energy Research (Capacity Area A3: Minimization of energy demand) for the financial support. This research also benefitted from support from the Swiss National Science Foundation within the framework of the National Center of Competence in Research for Bio-Inspired Materials. We would also like to thank

the Institute of Polymer Engineering at the FHNW University of Applied Sciences and Arts Northwestern Switzerland for kindly providing access to analytical equipment, Dr. Meike Heinz for the access to the iso-static press, Mr. Faruk Okur and Mr. Yannick Nagel for assisting with the experiments, as well as the Scientific Center for Optical and Electron Microscopy of ETH Zürich (ScopeM) for the access to the microscopes and the ion beam milling tool utilised in this work.

Author affiliations: [a]Complex Materials, Department of Materials, ETH Zürich, 8093 Zürich, Switzerland; [b]High Enthalpy Flow Diagnostics Group, Institute of Space Systems, University of Stuttgart, 70569 Stuttgart, Germany; and [c]Centre for Advanced Structural Ceramics, Department of Materials, Imperial College London, London, United Kingdom

Author contributions: K.M. and A.R.S. designed research; W.W., E.P., M.G., F.B., and K.M. performed research; E.P., M.G., and F.B. contributed new reagents/analytic tools; W.W., F.B., K.M., and A.R.S. analyzed data; and W.W., K.M., and A.R.S. wrote the paper.

1. A. P. Jackson, J. F. V. Vincent, R. M. Turner, The mechanical design of nacre. *Proc. R. Soc. London. B.* **234**, 415–440 (1988).
2. F. Barthelat, H. Tang, P. D. Zavattieri, C. M. Li, H. D. Espinosa, On the mechanics of mother-of-pearl: A key feature in the material hierarchical structure. *J. Mech. Phys. Solids* **55**, 306–337 (2007).
3. M. Sarikaya, I. A. Aksay, Nacre of abalone shell: A natural multifunctional nanolaminated ceramic-polymer composite material. in *Structure, Cellular Synthesis and Assembly of Biopolymers*, S. T. Case, Vol. **19** (Springer-Verlag Berlin Heidelberg GmbH, 1992). pp. 1–26.
4. J. D. Currey, Mechanical properties of mother of pearl in tension. *Proc. R. Soc. London B.* **196**, 443–463 (1977).
5. U. G. K. Wegst, H. Bai, E. Saiz, A. P. Tomsia, R. O. Ritchie, Bioinspired structural materials. *Nat. Mater.* **14**, 23–36 (2015).
6. A. R. Studart, Towards high-performance bioinspired composites. *Adv. Mater.* **24**, 5024–5044 (2012).
7. L. J. Bonderer, A. R. Studart, J. Woltersdorf, E. Pippel, L. J. Gauckler, Strong and ductile platelet-reinforced polymer films inspired by nature: Microstructure and mechanical properties. *J. Mater. Res.* **24**, 2741–2754 (2009).
8. L. J. Bonderer, A. R. Studart, L. J. Gauckler, Bioinspired design and assembly of platelet reinforced polymer films. *Science* **319**, 1069–1073 (2008).
9. R. Libanori, F. H. L. Münch, D. M. Montenegro, A. R. Studart, Hierarchical reinforcement of polyurethane-based composites with inorganic micro- and nanoplatelets. *Compos. Sci. Technol.* **72**, 435–445 (2012).
10. F. Barthelat, C. M. Li, C. Comi, H. D. Espinosa, Mechanical properties of nacre constituents and their impact on mechanical performance. *J. Mater. Res.* **21**, 1977–1986 (2006).
11. S. Askarinejad, N. Rahbar, Toughening mechanisms in bioinspired multilayered materials. *J. R. Soc. Interface* **12**, 20140855 (2015).
12. M. A. Meyers, A. Y. M. Lin, P. Y. Chen, J. Muyco, Mechanical strength of abalone nacre: Role of the soft organic layer. *J. Mech. Behav. Biomed. Mater.* **1**, 76–85 (2008).
13. M. Taniguchi, K. Fujita, M. Tsuji, I. Takewaki, Hybrid control system for greater resilience using multiple isolation and building connection. *Front. Built Environ.* **2**, 1–10 (2016).
14. M. D. Rao, Recent applications of viscoelastic damping for noise control in automobiles and commercial airplanes. *J. Sound Vibrat.* **262**, 457–474 (2003).
15. M. S. Seong, S. B. Choi, C. H. Kim, Damping force control of frictionless MR damper associated with hysteresis modeling. *J. Phys. Conf. Ser.* **412**, 012044 (2013).
16. A. Treviso, B. Van Genechten, D. Mundo, M. Tournour, Damping in composite materials: Properties and models. *Compos. Part B Eng.* **78**, 144–152 (2015).
17. E. Acar, M. Aydın, Damping behavior of Al/SiC functionally graded and metal matrix composites. *J. Asian Ceram. Soc.* **9**, 578–585 (2021).
18. D. D. L. Chung, Review: Materials for vibration damping. *J. Mater. Sci.* **36**, 5733–5737 (2001).
19. R. Bauri, M. K. Surappa, Damping behavior of Al-Li-Sicp composites processed by stir casting technique. *Metall. Mater. Trans. A.* **36**, 667–673 (2005).
20. S. Madeira, M. Gasik, J. C. M. Souza, F. S. Silva, B. Henriques, Damping and mechanical behavior of metal-ceramic composites applied to novel dental restorative systems. *J. Mech. Behav. Biomed. Mater.* **90**, 239–247 (2019).
21. X. Li *et al.*, Damping capacity and storage modulus of SiC matrix composites infiltrated by AlSi alloy. *Metals (Basel)* **9**, 1–11 (2019).
22. J. Zhang, R. J. Perez, C. R. Wong, E. J. Lavernia, Effects of secondary phases on the damping behaviour of metals, alloys and metal matrix composites. *Mater. Sci. Eng. Rep.* **13**, 325–389 (1994).
23. C. P. Chen, R. S. Lakes, Analysis of high-loss viscoelastic composites. *J. Mater. Sci.* **28**, 4299–4304 (1993).
24. A. P. Unwin *et al.*, Escaping the Ashby limit for mechanical damping/stiffness trade-off using a constrained high internal friction interfacial layer. *Sci. Rep.* **8**, 2454 (2018).
25. F. Duc, P. E. Bourban, C. J. G. Plummer, J.-E. Månson, Damping of thermoset and thermoplastic flax fibre composites. *Compos. Part A Appl. Sci. Manuf.* **64**, 115–123 (2014).
26. W. Woigk *et al.*, Bio-inspired platelet-reinforced polymers with enhanced stiffness and damping behavior. *ACS Appl. Polym. Mater.* **2**, 3557–3565 (2020).
27. B. Mohanty, K. S. Katti, D. R. Katti, D. Verma, Dynamic nanomechanical response of nacre. *J. Mater. Res.* **21**, 2045–2051 (2006).
28. T. Li, K. Zeng, Nanoscale elasticity mappings of micro-constituents of abalone shell by band excitation-contact resonance force microscopy. *Nanoscale* **6**, 2177–2185 (2014).
29. M. Brodt, R. S. Lakes, Composite materials which exhibit high stiffness and high viscoelastic damping. *J. Compos. Mater.* **29**, 1823–1833 (1994).
30. M. N. Ludwigson, R. S. Lakes, C. C. Swan, Damping and stiffness of particulate SiC-InSn composite. *J. Compos. Mater.* **36**, 2245–2254 (2002).
31. M. Barrado, G. A. López, M. L. Nó, J. San Juan, Composites with ultra high damping capacity based on powder metallurgy shape memory alloys. *Mater. Sci. Eng. A* **521–522**, 363–367 (2009).
32. P. Zhang, A. C. To, Highly enhanced damping figure of merit in biomimetic hierarchical staggered composites. *J. Appl. Mech.* **81**, 051015 (2014).
33. L. Dong, C. Chao, P. Yan, Effective modulus of biological staggered nanocomposites with interface stress effect. *Compos., Part B Eng.* **166**, 701–709 (2019).
34. J. Liu, X. Hai, W. Zhu, X. Wei, Optimization of damping properties of staggered composites through microstructure design. *J. Appl. Mech.* **85**, 101002 (2018).
35. M. Qwamizadeh, K. Zhou, Y. W. Zhang, Damping behavior investigation and optimization of the structural layout of load-bearing biological materials. *Int. J. Mech. Sci.* **120**, 263–275 (2017).
36. M. Grossman *et al.*, Mineral nano-interconnectivity stiffens and toughens nacre-like composite materials. *Adv. Mater.* **29**, 1605039 (2017).
37. R. M. Erb, R. Libanori, N. Rothfuchs, A. R. Studart, Composites reinforced in three dimensions by using low magnetic fields. *Science* **335**, 199–205 (2012).
38. R. M. Erb, J. Segmehl, M. Schaffner, A. R. Studart, Temporal response of magnetically labeled platelets under dynamic magnetic fields. *Soft Matter* **9**, 498–505 (2013).
39. R. M. Erb, J. Segmehl, M. Charilaou, J. F. Löffler, A. R. Studart, Non-linear alignment dynamics in suspensions of platelets under rotating magnetic fields. *Soft Matter* **8**, 7604–7609 (2012).
40. M. Grossman, F. Bouville, K. Masania, A. R. Studart, Quantifying the role of mineral bridges on the fracture resistance of nacre-like composites. *Proc. Natl. Acad. Sci. U.S.A.* **115**, 12698–12703 (2018).
41. P. Zhang, M. A. Heyne, A. C. To, Biomimetic staggered composites with highly enhanced energy dissipation: Modeling, 3D printing, and testing. *J. Mech. Phys. Solids* **83**, 285–300 (2015).
42. S. Cui, Z. Lu, Z. Yang, X. He, Numerical investigation on the enhanced damping behavior of bio-inspired nacreous composites by introducing interlocked structure. *J. Mech. Behav. Biomed. Mater.* **119**, 104442 (2021).
43. T. Magrini *et al.*, Transparent and tough bulk composites inspired by nacre. *Nat. Commun.* **10**, 2794 (2019).
44. T. Magrini *et al.*, Transparent nacre-like composites toughened through mineral bridges. *Adv. Funct. Mater.* **30**, 2002149 (2020).
45. R. S. Lakes, High damping composite materials: Effect of structural hierarchy. *J. Compos. Mater.* **36**, 287–297 (2002).
46. *CES EduPack* (Granta Design Limited, Cambridge, UK, 2017).
47. H.-C. Loh *et al.*, Nacre toughening due to cooperative plastic deformation of stacks of co-oriented aragonite platelets. *Commun. Mater.* **1**, 1–10 (2020).
48. G. X. Gu, M. Takaffoli, M. J. Buehler, Hierarchically enhanced impact resistance of bioinspired composites. *Adv. Mater.* **29**, 1700060 (2017).
49. G. X. Gu, F. Libonati, S. D. Wettermark, M. J. Buehler, Printing nature: Unraveling the role of nacre's mineral bridges. *J. Mech. Behav. Biomed. Mater.* **76**, 135–144 (2017).
50. K. Guo, Z. Yang, C. H. Yu, M. J. Buehler, Artificial intelligence and machine learning in design of mechanical materials. *Mater. Horiz.* **8**, 1153–1172 (2021).
51. J. Schindelin *et al.*, Fiji: An open-source platform for biological-image analysis. *Nat. Methods* **9**, 676–682 (2012).
52. T. Hildebrand, P. Rüegsegger, A new method for the model-independent assessment of thickness in three-dimensional images. *J. Microsc.* **185**, 67–75 (1997).